The Analysis Of Time Series And Frequency Data From Engineering Applications

Sandra Nahmia Wesly Aziz

Born 25^{th} May 1997 in Asiut, Egypt

2nd December 2019

Bachelor's Thesis Mathematics

Advisor: Prof. Dr. Jochen Garcke

Second Advisor: Dr. Sebastian Mayer

Institut für Numerische Simulation

Mathematisch-Naturwissenschaftliche Fakultät der

Rheinischen Friedrich-Wilhelms-Universität Bonn

Acknowledgement

First of all, I would like to thank Prof.Dr. Jochen Garcke for granting me the opportunity to work in his research group, for his interest and help. I also deeply thank my supervisor Dr. Sebastian Mayer for his guidance, support and patience throughout the whole duration. Many thanks to my internal supervisor Prof.Dr. Gerd Baumann for his interest and support.

Also I would like to thank The German University in Cairo for granting me the scholarship for conducting my Bachelor Thesis in Germany.

Contents

Chapter 1

Introduction

Anomaly detection is one of the main goals of data science. It is the attempt to detect the data points with substantial variations from the norm in a data set [MMH17]. Depending on the type of the data set under inspection, an anomaly could indicate different events, for example, an anomaly in a bank account transactions could indicate a theft or a fraud. On the other hand, in the case of vibration spectra an anomaly could indicate the presence of a mass imbalance. From a statistical point of view the data is assumed to follow a certain distribution. Fitting a model to this distribution, anomalies could then be identified as data points that don't fit well to the model [ZS17].

The data used in this project is from Blade Control for wind energy plants(WEP), where each WEP has 6 sensors, 2 on each blade to record edge-wise and flap-wise vibrations. The data is given in the form of spectra, i.e. the Fast Fourier Transform is already calculated for the time domain vibrational amplitudes.

The data used in this project was grouped in two sets:

1. **25 WEP Data Set**
   This data set includes spectra for low vibration frequencies for 25 WEPs. The measurements were recorded over 4 years using two sensors for each blade to record edge-wise and flap-wise vibrations. The data set was used for explorative analysis of Campbell diagrams.

2. **Anomaly Data Set**
   This dataset includes spectra for high vibration frequencies for 1 WEP. The measurements were recorded over 7 months and an anomaly was reported at the end of the fifth month. The WEP was then turned of to fix the damage and was restarted again with different operation conditions. This data set was used to investigate the possibility of using Campbell diagrams as features for anomaly detection.

Due to the large number of spectra and the high noise levels in them, the attempt to fit a model for a single spectrum is very complicated, especially when the important features characterizing the spectra are not clearly defined. Figure 1.1 shows a single spectrum of a vibrational frequency across time, it gives an insight on how irregular the spectra could be, for example, the real peaks can't be distinguished from noise artifacts.

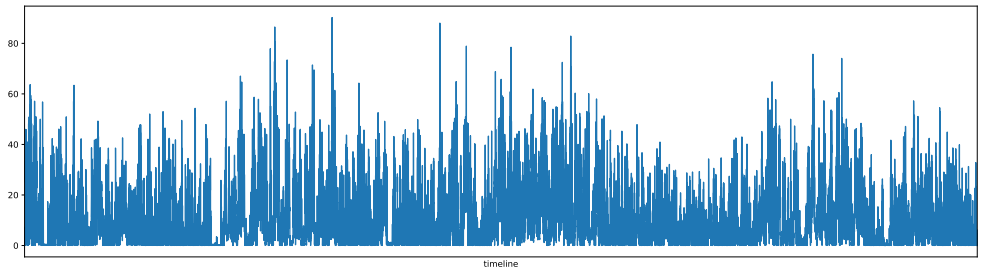

Figure 1.1: A spectrum of a single vibrational frequency.

Spectrograms (intensity plots, usually in a logarithmic scale, of a collection of spectra [Smi15]) are then plotted, where the $x-axis$ is the rotational frequencies of the blades and the $y-axis$ is the vibrational frequencies. For a rotational structure these spectrograms are known as Campbell Diagrams. Campbell diagrams increase the signal to noise ratio and eliminate the main source of spectral variations, the rotational frequency. These were the main motives to study Campbell diagrams as the starting point for anomaly detection.

The main features in the Campbell diagrams are horizontal and diagonal straight lines which form from the alignment of the important peaks of different spectra. However, the noise in the spectra also contributes to the collective spectrograms, resulting in fake peaks and artifacts in the Campbell diagrams. This made the traditional edge detection operators not useful. The first research topic this thesis examines, is line extraction from Campbell diagrams using Radon transform and Hough transform.
Campbell diagrams, along with the results of adjusted line transforms, were then visually analyzed in order to investigate which features or lines could be used for anomaly detection, which is the second research topic of this thesis.

Chapter 2 introduces the theoretical and mathematical background. It gives a quick overview of the vibrational analysis of wind turbines and Campbell diagrams; it also explains the principles of traditional edge detectors and the mathematical formulation of Radon and Hough transforms, which will later be used for line detection in Campbell diagrams. Finally, it presents a brief overview on wavelet transform which will be used in the anomaly detection method.

Chapter 3 presents the process of detecting the horizontal and diagonal lines in Campbell diagrams. First, the effects of noise on traditional edge detection operators are discussed. Then, Radon transform was proposed as a line detection method that is more robust against high noise levels. Changes were then applied to Radon transform in order to make it more suitable for line detection in Campbell diagrams. Finally, Hough transform is also proposed as a suitable line detection method after applying some adjustments to it.

Chapter 4 presents the analysis of Campbell diagrams for the two datasets. For the first data set, explorative analysis was done to roughly determine the shortest time period to produce useful Campbell diagrams and to visually explore the interesting phenomena in the Campbell diagrams and the potential features that could be used for anomaly detection. For the second data set, the passibility

to use the results of the adjusted Radon and Hough transforms as features for early damage detection in a wind turbine using wavelet transform was explored.

Finally, chapter 5 presents the conclusion and future recommendations for using Campbell diagrams as features for anomaly detection.

Chapter 2

Background

2.1 Vibration Analysis Of Wind Turbines

The slender and elastic construction of modern wind turbines makes them extremely prone to vibration [Hau13]. Vibration analysis of wind turbines aims for identifying the most dangerous rotational frequencies, at which resonance occurs; hence, ascertain the dynamic stability within the permissible range of operation frequencies. Vibrational complications in wind turbines can originate in many parts of the structure. For example, the slender rotor blades are subjected to aeroelastic influences. Also, the whole structure, i.e. the rotor/tower-system, can vibrate.

The vibration of the whole system, or some of the subsystems, is triggered by internal or external **Excitation Forces**.
Some of the external forces(cyclically alternating forces) are :

- **Mass imbalances of the rotor**, which can happen due to manufacturing defects in the rotor blades, or due to accumulation of ice on the blades.
- **Tower wind shadow effect**, which is the shock impact on each rotor blade upon passing by the tower, as in that instant the wind current, perpendicular to the rotor blades, abruptly vanishes.

Examples of internal forces are:

- **Meshing Gear Frequencies**, which result from imperfect or broken teeth within the gear boxes.
- **Electrical Grid Oscillations**, when grid feed lines are excessively long.

Some of the previous events are inevitable, for example, the tower wind shadow effect will always exist as long as the blades are rotating, implying that eventually the wind turbine will be excited into vibrational motion.

Each subsystem of the wind turbine has some **Natural(Eigen) Frequencies**. If the system was excited at these frequencies, resonance occurs. The most important step in vibration analysis is to make sure that, inside the operation range of the wind turbine, an excitational force does not excite one of

the systems natural frequencies. However, not all the correspondences between the excitational forces and the natural frequencies are equally dangerous. If the excitation frequency coincides with the natural frequency of a mode(subsystem) that is completely uncoupled with it, no resonance actually occurs. In other cases, the resonance can be very weak that the damping forces of the system can be sufficient to avoid any damage [Gen09]. Rotational frequencies at which an excitation force coincide with a natural frequency are called **Critical Frequencies**.

2.2 Campbell Diagrams

Normally the vibrational analysis of a rotor is performed under the assumption of constant rotational frequency, or at least constant average value. However, natural frequencies of a deformable rotor or, more generally, a deformable structure containing the rotor, can vary with the rotational frequency. As a result, the system response is summarized in a plot of the natural frequencies as functions of rotational frequencies [Gen09].
A rotor is also susceptible to external and internal excitation forces which are plotted as diagonal lines passing through the origin. The complete plot of the system response, including both natural frequency lines and excitation forces, is called the **Campbell Diagram** of the system. Fig.2.1a shows an idealized Campbell diagram, where the $x - axis$ is the rotational frequency(Hz) and the $y - axis$ is the vibrational frequency(Hz).
Campbell diagrams are line-based diagrams, the presence of certain lines with certain slopes, or a shift in the lines locations, indicates the occurrence of certain phenomena. Nevertheless, one phenomenon can result in more than one line, with slopes that are integer multiples of each other. These are known as **Harmonics**.

In the case of wind turbines, the eigen frequencies of the structure are nearly constant with respect to the rotational frequency, therefore, they are plotted as horizontal lines while the excitation forces are plotted as diagonal lines passing through the origin, with different slopes depicting different triggering factors.
Diagonal lines that are due to external factors occur at slopes of integer multiples of the rotational frequencies. For instance, lines due to mass imbalances of the rotor blades have slopes of 1P(per revolution), while lines depicting the tower wind shadow occur at slopes of nP(where n is the number of rotor blades of the wind turbine). The data used in this project is measured from a 3-blade system, so these lines occur at slopes 3P, 6P, ... On the other hand, diagonal lines due to internal factors have higher slopes; the meshing frequency lines have slopes dependent on the number of teeth in the gears.
Critical frequencies in a Campbell diagram are frequencies at which a diagonal line intersects with a horizontal line; in fig. 2.1a, the first meshing gear frequency excites the system second eigen frequency inside the operation range. One of the major disadvantages of the Campbell Diagrams is that they don't differentiate between important(dangerous) intersections and non important ones.

Typically a Campbell diagram is plotted after the analysis of the system.

First, the natural frequencies of the structure and the excitation forces are approximately calculated, then they are reported on the plot known as Campbell diagram. In this project, Campbell diagrams are plotted using real spectra measured from vibrational sensors.
Figure 2.1b shows a Campbell diagram plotted using the real measuring data, where the white regions are missing measurements at the corresponding rotational frequencies. It is clear that the Campbell diagram generated from real spectra is very noisy and the lines are not clear, which makes line detection a more challenging problem.

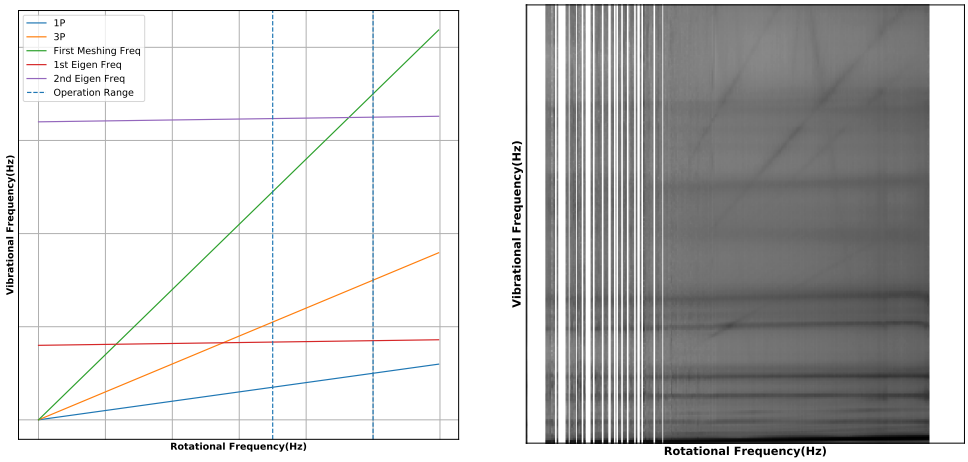

(a) Idealized Campbell diagram.

(b) Real Campbell diagram.

Figure 2.1: Campbell Diagrams.

2.3 Edge Detection

Edge detection is the process of defining the boundaries between different areas in the image. Edges could also be the contours that define geometric shapes.
In digital images, edges are set of pixels, where abrupt changes in the color intensity take place that result in critical points in the gradient of the intensity function of the digital image at those pixels or a zero crossing in the second order derivative of the same function . Most traditional edge detectors are based on those two principles [**?**].

Let the intensity of the image at each pixel (x, y) be given by the function $f(x, y)$, where x and y are the rows and columns respectively. The gradient then can be estimated using the finite difference method:

$$\frac{\partial f}{\partial x} = \lim_{h \to 0} \frac{f(x+h, y) - f(x, y)}{h}$$
$$\frac{\partial f}{\partial y} = \lim_{h \to 0} \frac{f(x, y+h) - f(x, y)}{h}$$

which can be approximated by:

$$\frac{\partial f}{\partial x} \approxeq \frac{f(x+h,y)-f(x,y)}{h}|_{h=1} = f(x+1,y)-f(x,y) \tag{2.1}$$

$$\frac{\partial f}{\partial y} \approxeq \frac{f(x+h,y)-f(x,y)}{h}|_{h=1} = f(x+1,y)-f(x,y) \tag{2.2}$$

Another approach for approximating the gradient is using a convolution kernel, the image is convolved with a mask(matrix) that has the same effect as eqs. (2.1) and (2.2):

$$\frac{\partial f}{\partial x} \approxeq \begin{bmatrix} 0 & 0 & 0 \\ 0 & -1 & 0 \\ 0 & 1 & 0 \end{bmatrix} = \begin{bmatrix} -1 \\ 1 \end{bmatrix} \qquad \frac{\partial f}{\partial y} \approxeq \begin{bmatrix} 0 & 0 & 0 \\ 0 & -1 & 1 \\ 0 & 0 & 0 \end{bmatrix} = \begin{bmatrix} -1 & 1 \end{bmatrix}$$

Some examples of the gradient based edge detectors:

1. **Roberts Edge Detector**
   It implements Roberts Cross Gradient Operator:

$$\frac{\partial f}{\partial x} = f(x+1,y+1)-f(x,y)$$
$$\frac{\partial f}{\partial y} = f(x,y+1)-f(x+1,y)$$

   or using the convolution mask:

$$\frac{\partial f}{\partial x} = \begin{bmatrix} 0 & 0 & 0 \\ 0 & -1 & 0 \\ 0 & 0 & 1 \end{bmatrix} = \begin{bmatrix} -1 & 0 \\ 0 & 1 \end{bmatrix} \qquad \frac{\partial f}{\partial y} = \begin{bmatrix} 0 & 0 & 0 \\ 0 & 0 & -1 \\ 0 & 1 & 0 \end{bmatrix} = \begin{bmatrix} 0 & -1 \\ 1 & 0 \end{bmatrix}$$

   Roberts edge detector has the shortest support which makes it very prone to noise and can only detect sharp edges; however, it detects the edges' position with high accuracy.

2. **Prewitt Edge Detector**
   This edge detector has a longer support so it is more robust against noise, but it detects the edges' positions with lower accuracy.
   The Partial derivatives are calculated by:

$$\begin{aligned} \frac{\partial f}{\partial x} &= (f(x+1,y-1)+f(x+1,y)+f(x+1,y+1)) \\ &\quad -(f(x-1,y-1)+f(x-1,y)+f(x-1,y+1)) \\ \frac{\partial f}{\partial y} &= (f(x-1,y+1)+f(x,y+1)+f(x+1,y+1)) \\ &\quad -(f(x-1,y-1)+f(x,y-1)+f(x+1,y-1)) \end{aligned}$$

   or using the convolution mask:

$$\frac{\partial f}{\partial x} = \begin{bmatrix} -1 & -1 & -1 \\ 0 & 0 & 0 \\ 1 & 1 & 1 \end{bmatrix} \qquad \frac{\partial f}{\partial y} = \begin{bmatrix} -1 & 0 & 1 \\ -1 & 0 & 1 \\ -1 & 0 & 1 \end{bmatrix}$$

3. Sobel Edge Detector

The only difference between the Sobel operator and the Prewitt operator is the weight of the center coefficient(which is 2 in the Sobel operator and 1 in the Prewitt operator). This gives the Sobel operator better noise suppression characteristics [Cha05].

The partial derivatives are calculated by:

$$\begin{aligned}\frac{\partial f}{\partial x} &= (f(x+1,y-1)+2f(x+1,y)+f(x+1,y+1))\\ &\quad -(f(x-1,y-1)+2f(x-1,y)+f(x-1,y+1))\\ \frac{\partial f}{\partial y} &= (f(x-1,y+1)+2f(x,y+1)+f(x+1,y+1))\\ &\quad -(f(x-1,y-1)+2f(x,y-1)+f(x+1,y-1))\end{aligned}$$

or using the convolution mask:

$$\frac{\partial f}{\partial x} = \begin{bmatrix}-1 & -2 & -1\\ 0 & 0 & 0\\ 1 & 2 & 1\end{bmatrix} \qquad \frac{\partial f}{\partial y} = \begin{bmatrix}-1 & 0 & 1\\ -2 & 0 & 2\\ -1 & 0 & 1\end{bmatrix}$$

Sometimes the image is convolved with a Gaussian kernel first, to decrease the effect of noise before calculating the gradient of the image, $\frac{\partial(G*f)}{\partial x}$, but since both operations are convolutions, and convolution is associative, the derivative kernel is first convolved with a Gaussian kernel and the resultant is then convolved with the image, $f * (\frac{\partial G}{\partial x})$, [FP12].

Another edge detection algorithm is Canny, which uses a multistage algorithm to detect wide range of edges in images [SKN16]:

1. Smooth the image with a Gaussian filter.
2. Compute the gradient magnitude (using one of the previous operators).
3. Edge thinning by applying non-maximum suppression.
4. Apply double threshold to determine potential edges.
5. Track edges by hysteresis.

The operator used in the type of edge detectors based on the second principle, the presence of a zero crossing in the second order derivative, is called Laplacian of the Gaussian(LOG) operator. The Laplacian operator is applied to the Gaussian kernel, to smooth any discontinuities, and the resultant kernel is convolved with the image. The pixels which have a zero value are considered edges. Figure 2.2 shows an example of a 1-D edge and the result of applying different operations on it.

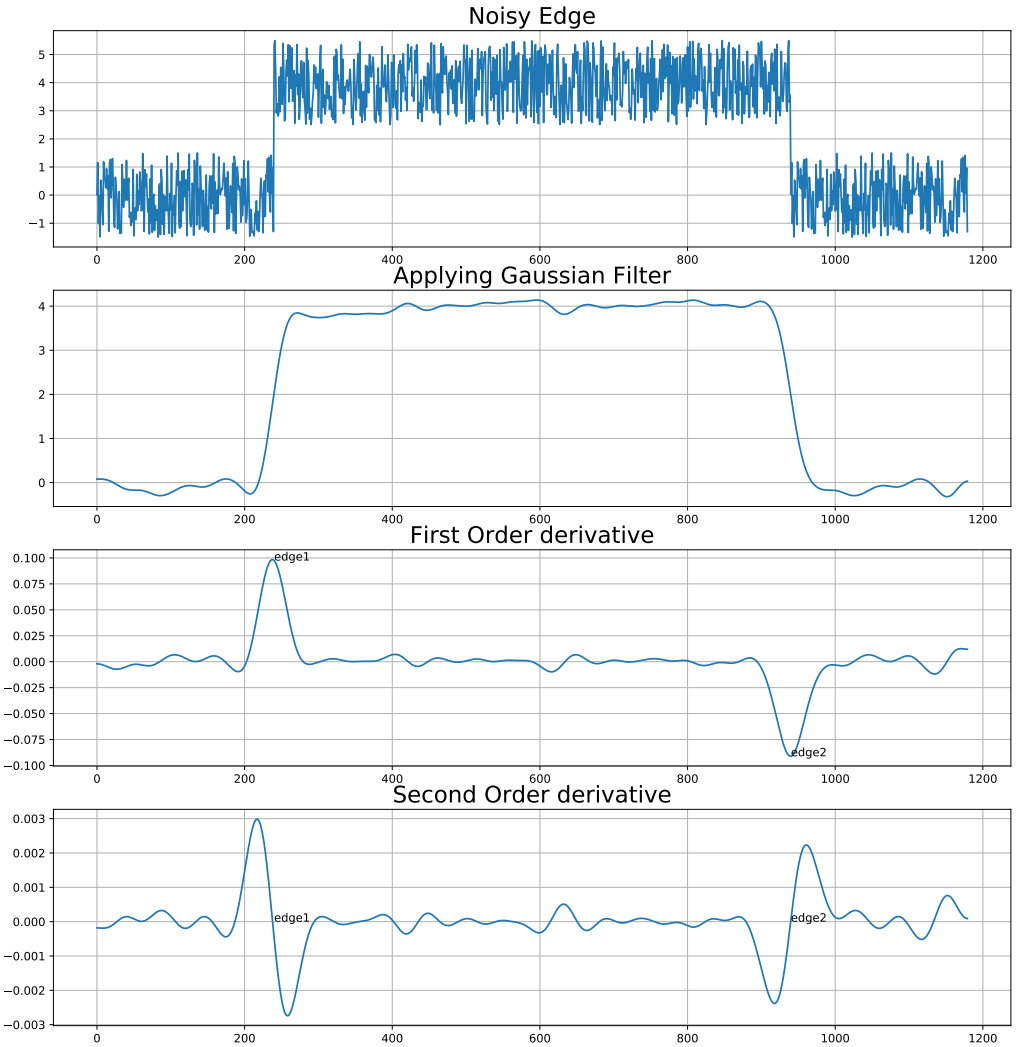

Figure 2.2: 1-D noisy edges, applying a gaussian filter to eliminate noise and calculating the first and second derivatives to detect the edges.

2.4 Radon Transform

2.4.1 Integral Transform

An Integral transform is a mathematical transform, that maps a function from its original domain to another domain, where it becomes easier to manipulate or solve. After performing the necessary operations on the function, the solution may be mapped again to the original domain using the Inverse transform [int]. The equation

$$g(x) = \int_a^b K(x,y)f(y)dy$$

is called a **Fredholm Equation of the First Kind** or an **Integral Transform**. The bi-variate function $K(x,y)$ is called the kernel function of the integral transform and is assumed to be defined and continuous on $a \leqslant x \leqslant b$ and $a \leqslant y \leqslant b$ [RHB06]. An example of integral transforms, is the **Laplace Transform** which maps a function from time domain (t) to frequency domain (s). In Laplace transform the Kernel function is $K(s,t) = e^{-st}$ and the integration limits are 0 and $+\infty$ where:

$$\mathcal{L}f(t) = \int_0^\infty f(t)e^{-st}dt$$

2.4.2 Straight Line Parametrization

A straight line in $\mathbb{R}^2$ can be defined by the equation $y = mx + b$, where m is the slope of the line and b is the $y - intercept$. However, a problem arises with this representation, the slope of a vertical line approaches infinity. Another representation is $\rho = x\cos(\phi) + y\sin(\phi)$, where ρ is the norm from the origin to the straight line and ϕ is the angle between this norm and the $(+ve)$ $x - axis$.

Consider a straight line L in the xy plane with norm=ρ and angle=ϕ, rotating the xy coordinates by angle ϕ, where the new coordinates are called ρ and s respectively, fig. 2.3.
Expressing the old coordinates (x,y) in terms of the new ones [Dea07]:

$$x = \rho\cos(\phi) - s\sin(\phi) \tag{2.3}$$
$$y = \rho\sin(\phi) + s\cos(\phi) \tag{2.4}$$

2.4.3 Radon transform Definition

Radon Transform was introduced in 1917 by Johann Radon [Rad86].

Theorem 1 *For all real points P=$[x,y]$ let $f(x,y)$ be a real function satisfying the following regularity conditions:*

1. *$f(x,y)$ is continuous;*
2. *The double integral,*

$$\int\int \frac{|\ f(x,y)\ |}{\sqrt{x^2+y^2}}dxdy \tag{2.5}$$

extending over the whole plane, converges;

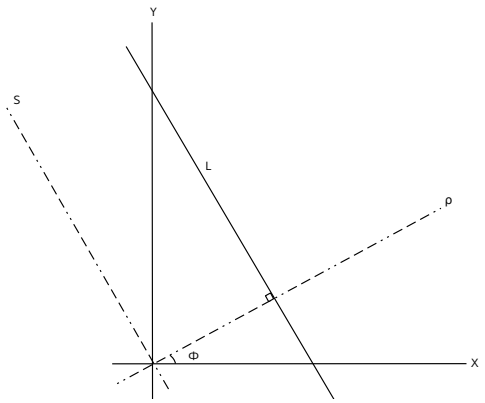

Figure 2.3: Rotating the original coordinates by ϕ.

3. *For an arbitrary point P=*$[x, y]$ *and each r⩾0*
   let

$$\bar{f}_p(r) = \frac{1}{2\pi} \int_o^{2\pi} f(x + r\cos\phi, y + r\sin\phi) d\phi$$

   so that for a point P

$$\lim_{r\to\infty} \bar{f}_p(r) = 0 \tag{2.6}$$

Then the following statement holds true: The straight line integral value of f along the line defined by the equation $\rho = x\cos(\phi) + y\sin(\phi)$ *is given by*

$$F(\rho, \phi) = F(-\rho, \phi + \pi) \quad = \quad \int_L f(x, y) ds \tag{2.7}$$

where ds is the increment along the line L. Using the transformation eqs. (2.3) *and* (2.4)*, eq.* (2.7) *becomes*

$$F(\rho, \phi) \quad = \quad \int_{-\infty}^{\infty} f(\rho\cos(\phi) - s\sin(\phi), \rho\sin(\phi) + s\cos(\phi)) ds \tag{2.8}$$

and exists almost everywhere; this means that on every circle the set of tangency points of all tangents for which F does not exist, has a linear measure of zero.

The assertions of Theorem 1 follow from known properties of absolutely convergent double integrals, which ascertain the existence of Radon transform at every point in the Campbell diagrams. However, they were never tested in our case because the amplitudes of the Campbell diagrams used vanish outside a certain range.

Now it can be deduced that 2-D Radon transform is a transform the maps a function f from 2-D space to the parametric space of straight lines. Figure 2.4 shows a graphical representation of the transform, where each line integral in the 2-dimensional space maps to a point in the radon space.

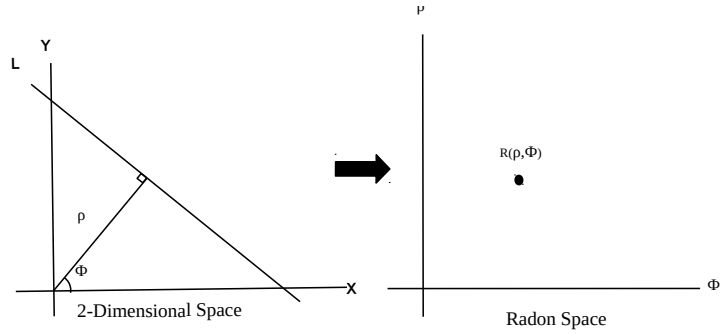

Figure 2.4: A line integral in the $\mathbb{R}^2$ domain maps to one point in the Radon space.

2.5 Hough Transform

Any mapping between two spaces can be approached from two perspectives. The first one is calculating the value of a point in the destination space from the source space, this is the approach used by Radon Transform ***(Line to Point Transform)***, where each line integral in $\mathbb{R}^2$ is the value of a point in the Radon space. The other perspective is calculating the contribution of each point in the source space to the value of all points in the destination space. This is the approach used by Hough Transform [GHV04].

Hough transform was originally used for line detection in binary black and white images. Like Radon, Hough transform is also a mapping function from the image space to a parametric line space. It also uses the same line parametrization used by Radon transform, that is each straight line is represented by the equation

$$\rho = x\cos(\phi) + y\sin(\phi) \tag{2.9}$$

where ρ is the normal distance between the line and the origin, while ϕ is the angle between this norm and the $(+ve)x - axis$.

At any pixel in the image the values of x and y are already known, while ρ and ϕ that satisfy eq. (2.9) are the unknown parameters we are looking for, where all the satisfying (ρ,ϕ) pairs, map to a curve in the Hough space, fig. 2.5 ***(Point to Curve Transform)***. Also the curves of collinear points in the image space intersect at one point (ρ,ϕ) in the Hough space, fig. 2.6, [hou].

The transform is calculated by quantizing the Hough space to discrete values of ρ and ϕ forming a 2-D accumulator. For each non zero pixel (x, y) in the image is discretized (ρ,ϕ) curve, then all the accumulator cells along this curve are incremented by one. Cells with high values in the accumulator indicate the presence of the corresponding line in the image, fig. 2.7.

Hough transform can be generalized to detect other shapes; Hence, it is more generic than Radon transform. For example, it can be used to detect the presence of circles using the parametric equation

$$(x - a)^2 + (y - b)^2 = r$$

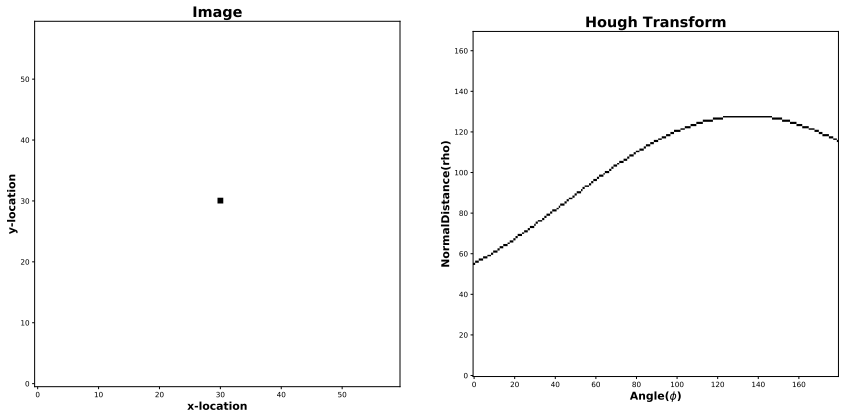

Figure 2.5: A point in the image space maps to a curve in the Hough space.

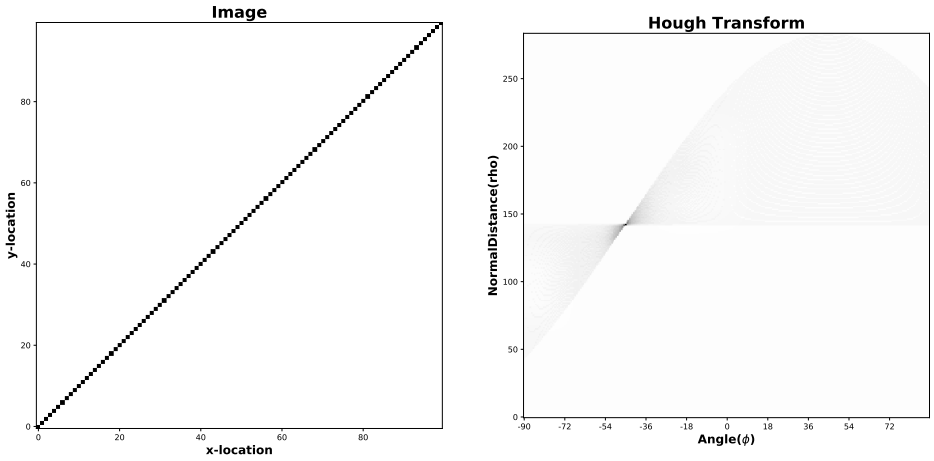

Figure 2.6: Collinear points in the image space intersects at a point in the Hough space.

where (a, b) is the centre of the circle and r is its radius. In this case the accumulator has three coordinates (a, b, r).
Hough transform can be further generalized to extract features that do not have simple parametric equations, in this case a look up table is used to define the relationship between the boundary positions and orientations and the Hough parameters.

2.6 Wavelet Transform

2.6.1 Fourier Transform and Short Time Fourier Transform

Fourier transform and its inverse are defined as:

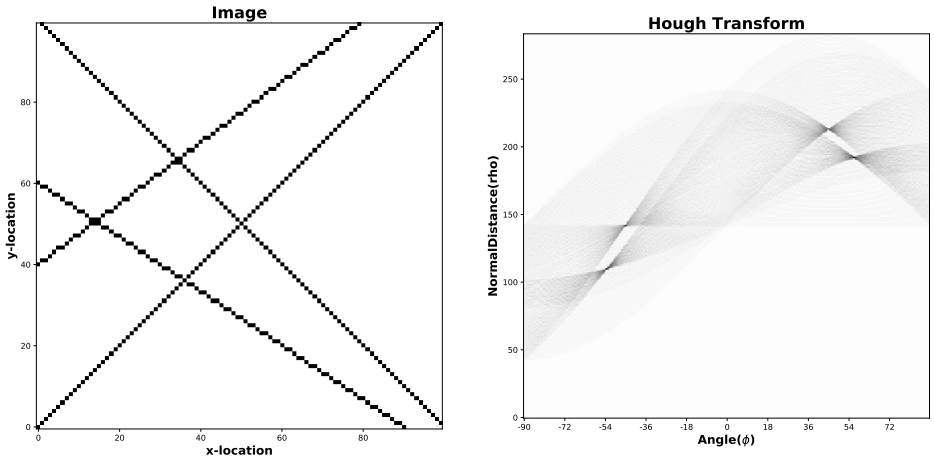

Figure 2.7: Hough Transform of an image. Lines in the image space maps to pixels with high intensity in the Hough space.

$$F(\omega) = \int_{-\infty}^{\infty} f(t) \exp(-j\omega t) dt \tag{2.10}$$

$$f(t) = \frac{1}{2\pi} \int_{-\infty}^{\infty} F(\omega) \exp(j\omega t) d\omega \tag{2.11}$$

Where $F(\omega)$ is the Fourier transform of the signal $f(t)$.
Using the identity:

$$\exp(jk\theta) = \cos(k\theta) + j \sin(k\theta) \tag{2.12}$$

eq. (2.11) becomes:

$$f(t) = \frac{1}{2\pi} \int_{-\infty}^{\infty} F(\omega) \cos(\omega t) + j \sin(\omega t) d\omega \tag{2.13}$$

Fourier transform $F(\omega)$ of a signal can then be seen as a function describing the contribution of sines and cosines to the construction of the original time domain signal. The time independence of the basis functions of the Fourier transform results in a signal description purely in the frequency domain, which makes it ideal for analysis of stationary signals whose statistical properties do not evolve over time [BM94].

For the analysis of non stationary signals a function is required that transforms a signal into a joint time-frequency domain. Such a description can be achieved using short time Fourier transform(STFT) defined by:

$$STFT(\tau, \omega) = \int s(t) g(t - \tau) \exp(-j\omega t) dt \tag{2.14}$$

which is the Fourier transform of the signal $s(t)$, previously windowed by the function $g(t)$ around the time τ.
As the window function is shifted in time over the whole signal and consecutive

overlapped transforms are performed, a description of the evolution of signal spectrum with time is achieved. However, as the length of the time window decreases to produce better time resolution, the frequency resolution also decreases(the uncertainty principle [BM94].).

2.6.2 Wavelet Transform and STFT

In eq. (2.10) the function $\exp(j\omega t)$ is called the basis function. In STFT the basis function is $g(t-\tau)\exp(-j\omega t)$. Thus eq. (2.14) can be written in a general form in terms of the basis function $K_{\tau,\omega}(t)$ and the signal $s(t)$:

$$STFT(\tau,\omega) = \int s(t)K_{\tau,\omega}(t)dt \tag{2.15}$$

The Wavelet Transform(WT) has the same concept as STFT except with different basis functions. The basis of the STFT are sines and cosines, which extend to infinity in time. However, the basis of the wavelet transform has compact support in time which makes them better in representing signals which has features with high amplitudes in short time.
Wavelet transform can also be described in terms of its basis function eq. (2.16):

$$\psi_{j,n}(t) = \frac{1}{\sqrt{2^j}}\psi(\frac{t-n}{2^j}) \tag{2.16}$$

where 2^j is the scaling factor and n is the time shift factor. Using eq. (2.15):

$$WT(n,j) = \int s(t)\psi_{j,n}(t)dt \tag{2.17}$$

From eq. (2.17) it can be seen that the WT performs a decomposition of the signal $s(t)$ into a weighted set of scaled wavelet functions $\psi(t)$.

The WT employs a set of basis functions that are scaled versions of a single "mother function", where wavelets at high frequencies are of limited duration and wavelets at low frequencies are relatively longer in duration. These variable window length characteristics are suited to the analysis of signals containing short high frequency components and extended low-frequency components, which is often the case for signals encountered in practice.

2.6.3 Wavelet Transform and Multiresolution analysis

The approximation of a function f at a resolution 2^{-j} is specified by a discrete grid of samples that provides local averages of f over neighbourhoods of size proportional to 2^j .The approximation of a function f at the resolution 2^{-j} is defined as the orthogonal projection $P_{V_j}f$ on V_j.
Adapting the signal resolution allows one to process only the relevant details for a particular task [Mal09].

Multiresolution approximations are entirely characterized by a particular discrete filter that governs the loss of information across resolutions. These discrete filters provide the procedure for designing and synthesizing orthogonal wavelet basis.

For $f \in L^2(\mathbb{R})$ the partial sum of wavelet coefficients $\sum_{n=-\infty}^{+\infty} < f, \psi_{j,n} > \psi_{j,n}$ can be interpreted as the difference between two approximations of f at the resolutions 2^{-j+1} and 2^{-j}.

Thus discrete wavelet transform serves as a decomposition method of signals at different resolutions, as the resolution increases, more fine and sharp details in the original signal are captured.

Chapter 3

Line Detection

As mentioned before, the main features in the Campbell diagrams are straight lines. This proposes that an anomaly most probably will appear in the Campbell diagram in the form of some changes in the lines. The first research topic this thesis examines, is line extraction from Campbell diagrams using Radon transform and Hough transform.

3.1 Effects of Noise

Usually the first step in line detection is edge detection. Most traditional edge detectors depend on the presence of critical points in the image gradient due to abrupt changes in the intensity of the image [Cha05], which makes them really simple and effective in detecting sharp edges with low noise levels which can be removed using Gaussian filters.

However, upon applying these edge detectors on the real data, one can observe that they do not produce clear edges, especially for the diagonal lines, fig. 3.1. The two main problems in our Campbell Diagrams which render the edge detection operators ineffective are:

1. **Smooth Edges**
   Traditional edge detectors work well when the difference between the edge pixels and the adjacent pixels is high(sharp edges). Sharp edges result in a single critical point in the first derivative, or a single zero crossing in the second order derivative, exactly at the edge location. But the edges present in the Campbell diagrams are very smooth resulting in a very smooth gradient.
   This problem is usually solved by using edge detectors with longer support, however, this significantly decrease the accuracy of the positions of the detected edges.

2. **High Noise Levels**
   Traditional edge detectors assume that the image has only small signal noise, that is the noise values oscillate with small amplitudes around the main amplitude of the signal.

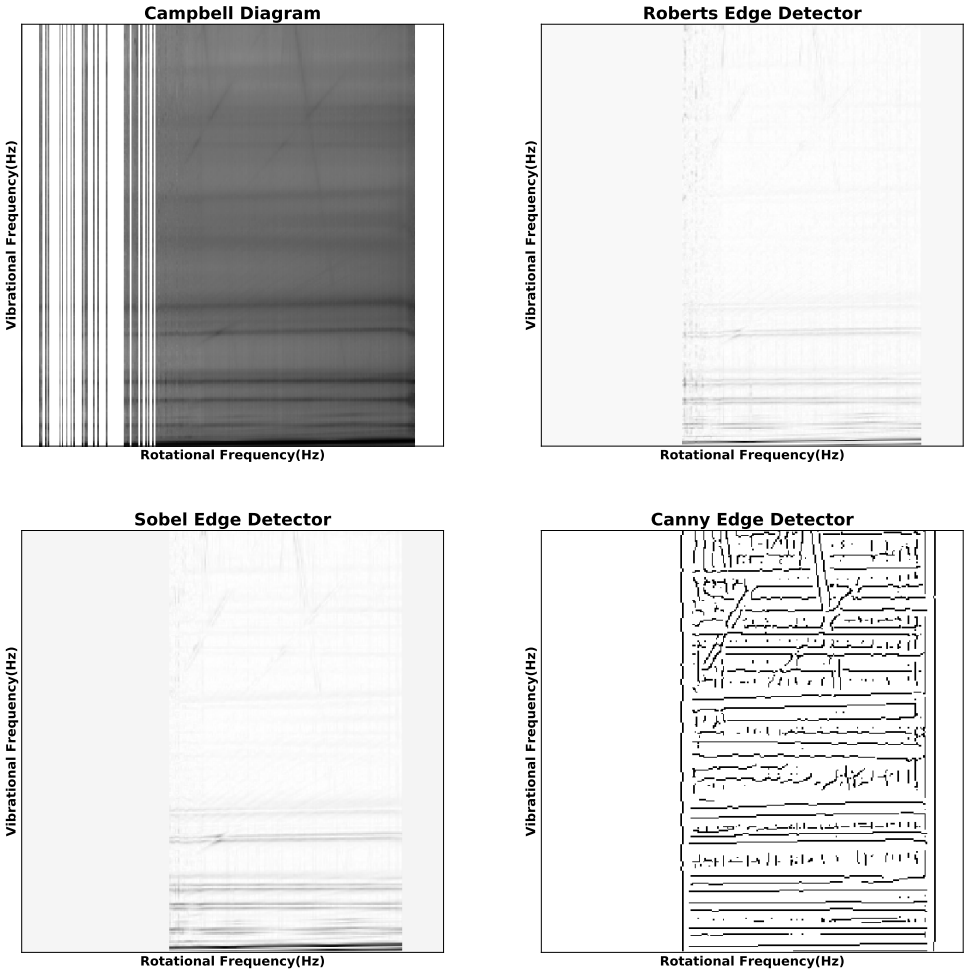

Figure 3.1: Results of applying traditional edge detectors to a real Campbell diagram.

This type of noise is easy to remove using a Gaussian filter or any other smoothing filter. However, the noise levels in the data are very high to the point that they can introduce fake peaks that, sometimes, are sharper and have the same intensity as real edges.

The main feature that defines the real peaks in a Campbell diagram is their alignment along certain contours. As a result we need a new edge or line detection algorithm that takes this feature into consideration.

3.2 Adjusted Radon transform

Radon transform, by definition, is the integration of a function along the set of all straight lines, which makes it very convenient for our purposes of line detection. It is not based on the intensity difference between the pixels, and as long as there are pixels with high intensities aligned along a line, a peak will

appear in the Radon transform. Even if the peak is not sharp, it is still possible to determine the location of the line with high accuracy. The integration also decrease the number of fake lines detected. For example, a peak resulting from ten pixels with very high intensities align along a line will still be low compared to a peak resulting from the alignment of a hundred pixels with high intensities. Thus, Radon transform solve both problems stated in the previous section.

Figure 3.2 shows the result of applying the Radon transform filter implemented in skimage library, where the output is a grey scale image with the angle ϕ and the distance ρ as the x and y axes respectively. Each pixel in the output image, $F(\phi, \rho)$, is the summation of pixel intensities in the source image along the straight line $\rho = x\cos(\phi) + y\sin(\phi)$. In fig. 3.2 the horizontal lines of the input Campbell diagram appear clearly as set of bold points at the center of the image ($\phi = 90°$). On the other hand, the diagonal lines can not be traced in the output. This is due to two main reasons:

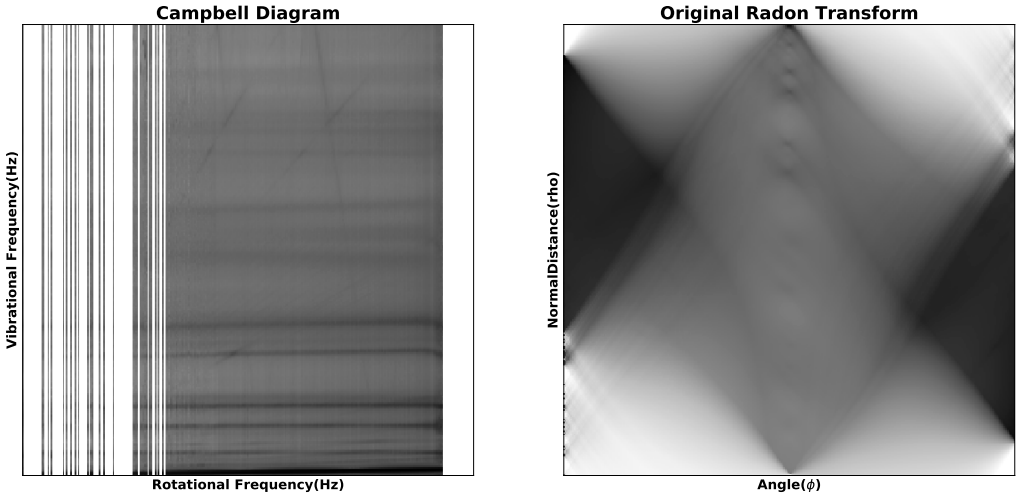

Figure 3.2: Result of applying original Radon transform algorithm on a real Campbell diagram.

1. The filter implementation define the origin at the centre of the image. Therefore, the peaks due to diagonal lines do not align along a certain contour in the output image. It was more convenient to define the origin at the corner($(0, 0)$point). Now the diagonal lines intensities is then given by the points with coordinates $(x, 0)$.

2. Compared with other lines in the image, the intensities of the diagonal lines are not significantly high, so the don't stand out upon plotting the complete transform. Usually we are only interested in a specific set of lines, either horizontal lines(eigen frequencies) or diagonal lines passing through the origin(excitation forces). In this case it is advantageous to calculate only partial transform, i.e. integrate only along certain set of lines.

The adjusted implementation, based on skimage implementation, of Radon transform is reported in Appendix A. Now the new output of the (partial) Radon

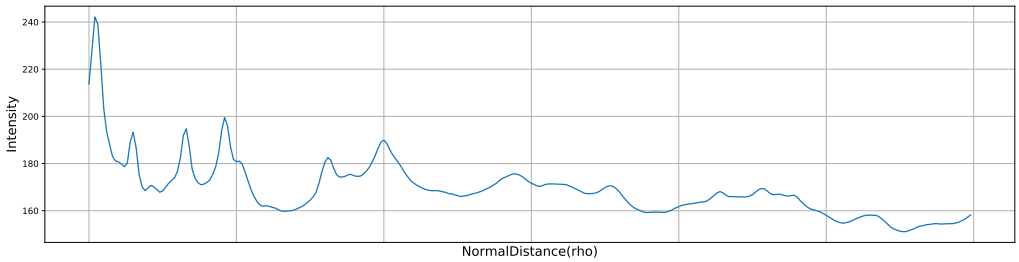

Figure 3.3: Result of applying adjusted Radon transform algorithm to detect horizontal lines on the same Campbell diagram.

transform is plotted as a curve, where the $x - axis$ is the angle between the diagonal line and the $(+ve)x - axis$ of the image (ϕ), in case of diagonal lines, or the distance from the origin, in case of horizontal lines(ρ), and the $y - axis$, in both cases, is the intensity of the line. Figure 3.3 shows the output of the adjusted Radon transform to detect horizontal lines for the same Campbell Diagram.

3.3 Adjusted Hough Transform

The close relation between Radon transform and Hough transform makes it a good candidate as a line detection algorithm for Campbell diagrams. Since Hough transform also does not depend on the gradient of the image, it avoids the problem of smooth edges and high noise levels. fig. 3.4 shows the result of applying the Hough transform filter implemented in skimage library. Originally, Hough transform was designed to detect lines in binary images. So in order to use it for grey scale images , edge detection algorithms should be used first. However, in our case, the better solution was to change the algorithm and instead of incrementing the cells of the accumulator by one for each non zero pixel, the accumulator is incremented by the value of the intensity of the pixel. Having done that, each pixel then contributes to the output with its intensity value; pixels with higher intensity have higher contribution. Another adjustment is applied on the transform, is restricting it to Diagonal lines, where the contribution of each pixel is calculated only for diagonal lines passing through the origin.

The adjusted Hough transform implementation is also reported in appendix A. The output of the adjusted Hough Transform has the same concept of adjusted Radon transform, where $x - axis$ is the angle and the $y - axis$ is the intensity, fig. 3.5.

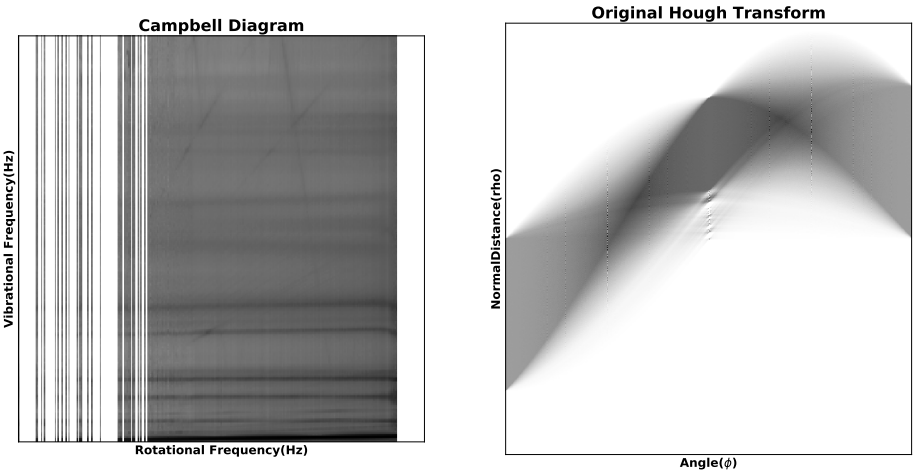

Figure 3.4: Result of applying original Hough transform algorithm on a real Campbell diagram.

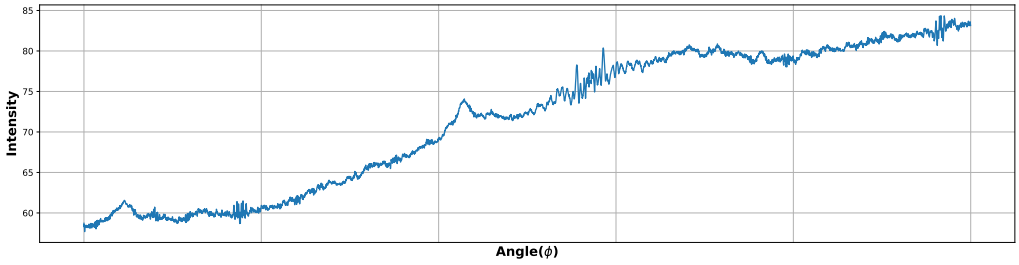

Figure 3.5: Result of applying adjusted Hough transform algorithm to detect diagonal lines on the same Campbell diagram.

Chapter 4

Analysis of Campbell Diagrams

4.1 Explorative Analysis

For the 25 WEP data set, a visual explorative analysis was done which aimed to answer two main research questions:

4.1.1 Shortest Time Period to Produce Useful Campbell Diagrams

Since the process of measurement was not based on the rotational frequency, but was periodic in time; The first step in the explorative analysis was finding the shortest time period to produce a useful Campbell Diagram.
The judging criteria was the percentage of the rotational frequencies, in the operation range, that exists in a time interval. High percentages means more frequencies in this interval and less gaps in the Campbell diagram.
The percentage was chosen based on the quality of the results produced by the line detection algorithms. Figure 4.1 shows the results of adjusted Hough transform for different sensors using Campbell diagrams with different percentages of rotational frequencies. In order for the transform to be stable, especially at higher angles, at least 80% of the rotational frequencies should exist.

Figure 4.2 plots a histogram of the length of the shortest time periods for the 25 Campbell diagrams.
The functions used to calculate the shortest time period is reported in Appendix A.

4.1.2 Interesting Phenomena in Campbell Diagrams

The second step in the explorative analysis, Campbell Diagrams were examined for uncommon phenomena. The data given was over the period of four years, so, it was first sectioned in spans of 12 months or 6 months.

Here is some of the observed phenomena and a brief explanation for each one:

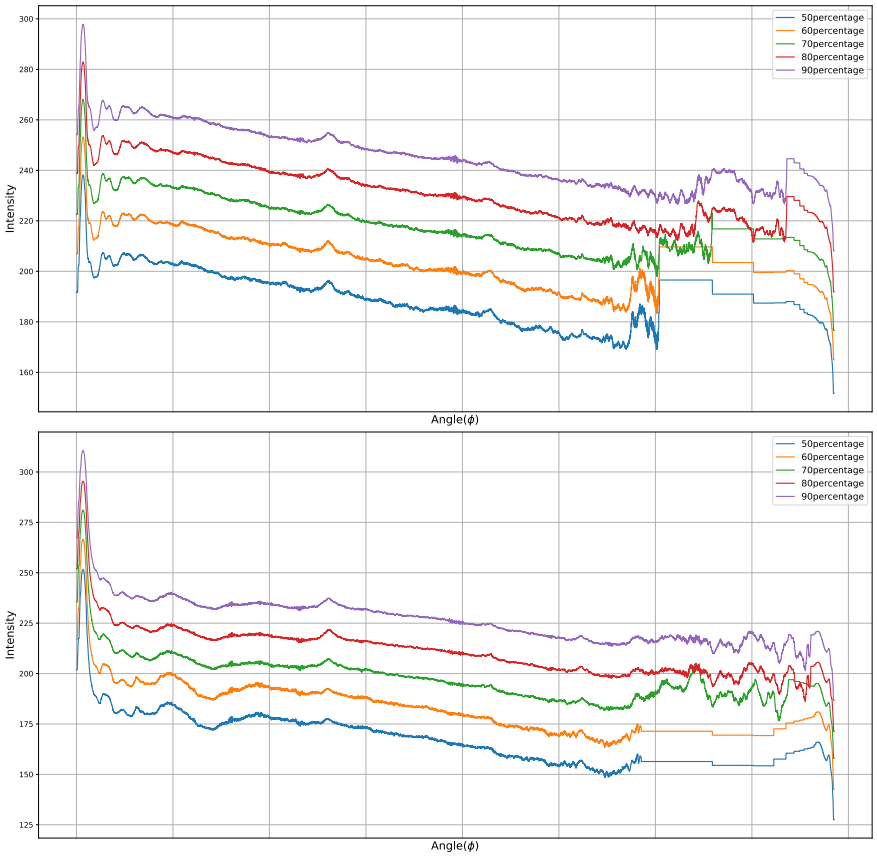

Figure 4.1: Adjusted Hough transform for different sensors using Campbell diagrams with different percentages of rotational frequencies.

Variation in the strength of excitation forces lines

This is the strongest observed phenomenon when comparing Campbell diagrams of different years for the same wind turbine. This phenomenon is interesting because the lines with high slopes mostly result from faulty gears and internal systems of the turbines, so they should not have higher intensity during on year then fade out during the next year. Figure 4.3a shows two Campbell diagrams(the diagrams on the right side are the same as the ones on the left side, only the important phenomena are highlighted), The fist Campbell diagram is plotted from data of an early year where the excitation forces lines are weak, while the second Campbell diagram is for a later year where the excitation forces are weaker. Figure 4.3b shows the intensity of the detected lines for the two years, where it is observed that at higher angles the peaks are higher.

Disappearance of a Natural Frequency

A natural frequency would completely disappear during one year then reappear again with the same intensity in the following year, fig. 4.4a.
This phenomenon is probably due to a shifting natural frequency. As a result of

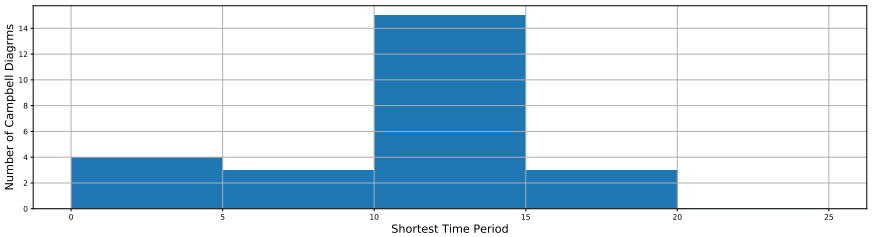

Figure 4.2: a Histogram of the length of the shortest time periods in days for the 25 Campbell diagrams.

the averaging during calculating the Campbell diagrams, this frequency appears twice and one of its versions appears and disappear, depending on the section of data used to plot the Campbell diagram. Figure 4.4b shows the intensity for the horizontal lines in the three time intervals.

Shifting Natural Frequencies

A slight downward shift, in the higher eigen frequencies is observed in most of the wind turbines from the winter period to the summer period of each year,fig. 4.5a. A downward shift in the natural frequency, theoretically, indicates the increase in the masses of the blades [Hau13]. This mass change could be a result of ice accumulation on the blades.

Negative Slope Line

In the Campbell diagrams of 10 out of the 25 wind turbines, a line with negative slope would appear, fig. 4.6. It appears more frequently in the Campbell diagrams generated from edge sensors vibrations than flap sensors vibrations. According to [Ehr08], this line appears due to a non-linear superharmonic response. This phenomenon is not normally reported in the literature of Campbell diagrams because, theoretically, they are plotted for linear systems or linearised model of the system. But since the Campbell Diagrams used in the analysis are plotted from real vibrational measurements, other non linear effects can also appear in them.

4.2 Anomaly Detection

For the anomaly data set, the goal was to detect if there were strong changes in the diagonal or horizontal lines in the Campbell diagrams before and after the anomaly. The anomaly is reported at the end of the fourth month, and the damage was repaired by the beginning of the sixth month. Figure 4.7 shows a sample Campbell diagram of one month, it can be observed that it has a lot of wide gaps due to missing measurements with respect to the rotational frequencies.

4.2.1 Visual Analysis for Anomaly Detection

In order to detect the anomaly two sets of lines were examined

Horizontal Lines (Eigen Frequency Lines) Plotting the intensity of horizontal lines at higher frequencies, fig. 4.8, it can be observed that across time some small peaks start to appear, also the shapes of other peaks changes.

Diagonal Lines (Excitation Forces) plotting the intensities of diagonal lines, it is observed that there is a peak which is present in the first five months, but disappears in the last two month when the anomaly is fixed, fig. 4.9

4.2.2 Anomaly Detection Using wavelet Transform

The next step in anomaly detection was trying to detect the changes in the horizontal lines across different months. Wavelet transform was used to construct the Radon transform for horizontal lines at high frequencies with certain number of layers. The error between the original signal and the constructed one was calculated. High error values indicates the presence of sharper details in the signal that requires higher wavelet scales to be captured. Table 4.1 shows a table with the month and the error in the constructed signal. It can be seen the the error decreases in the months before the anomaly but increases again after fixing the damage. An initial conclusion could be drawn from that observation that an anomaly shall change some of the peaks in the Campbell diagram to be more smooth and spread out. The algorithm used to calculate the error is reported in Appendix A. This approach, however, was ineffective with the other data set because only the low vibration frequencies existed.

Table 4.1: Table showing the error on each month upon using wavelet transform to reconstruct the Radon transform of Horizontal lines at higher frequencies

Month	Error
First Month	2822.51250885
Second Month	2380.34313806
Third Month	2101.95238226
Fourth Month	2270.4143543
Sixth Month	4576.75519968
Seventh Month	4255.30456401

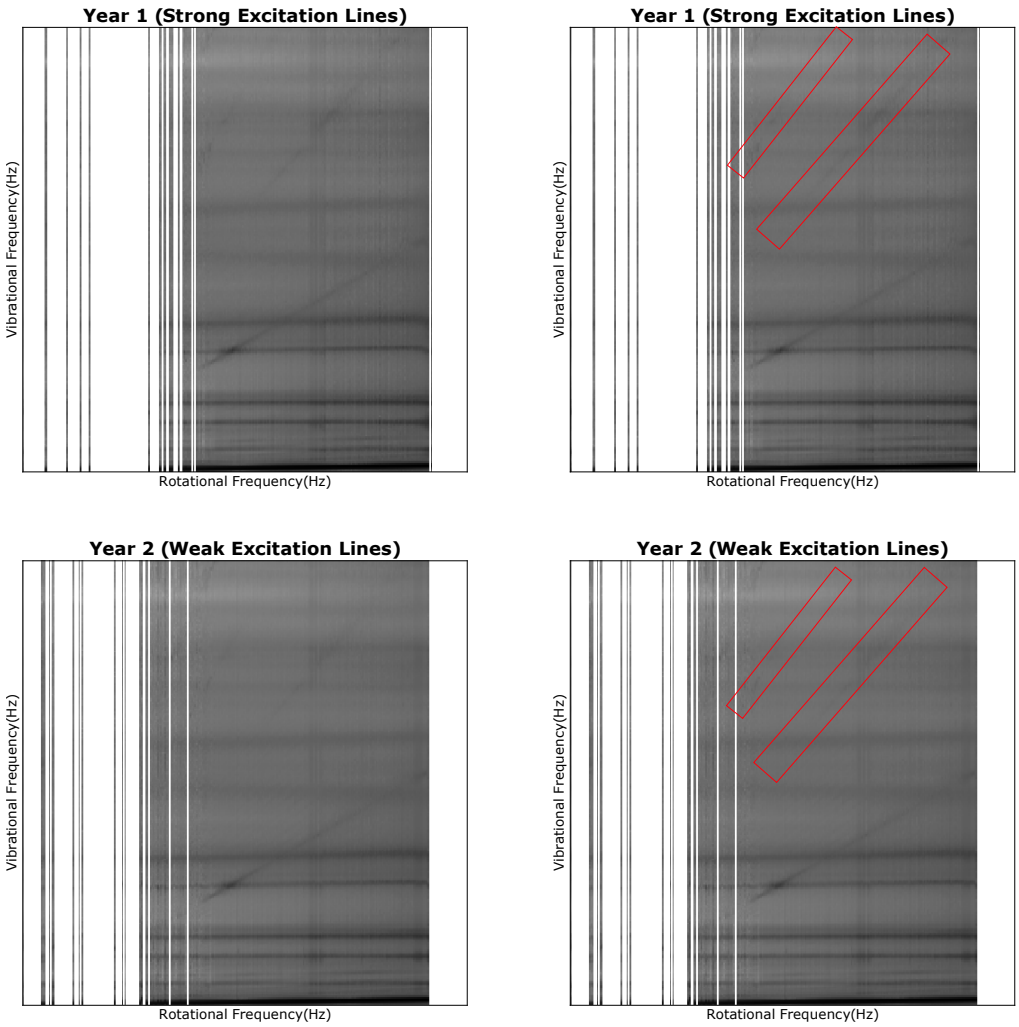

(a) Campbell diagrams Changing Strength of Diagonal Lines.

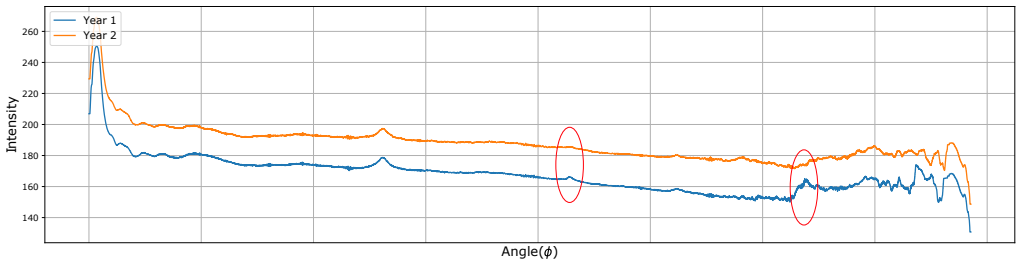

(b) Diagonal lines intensities for the two years.

Figure 4.3: Variation in the strength of excitation forces lines

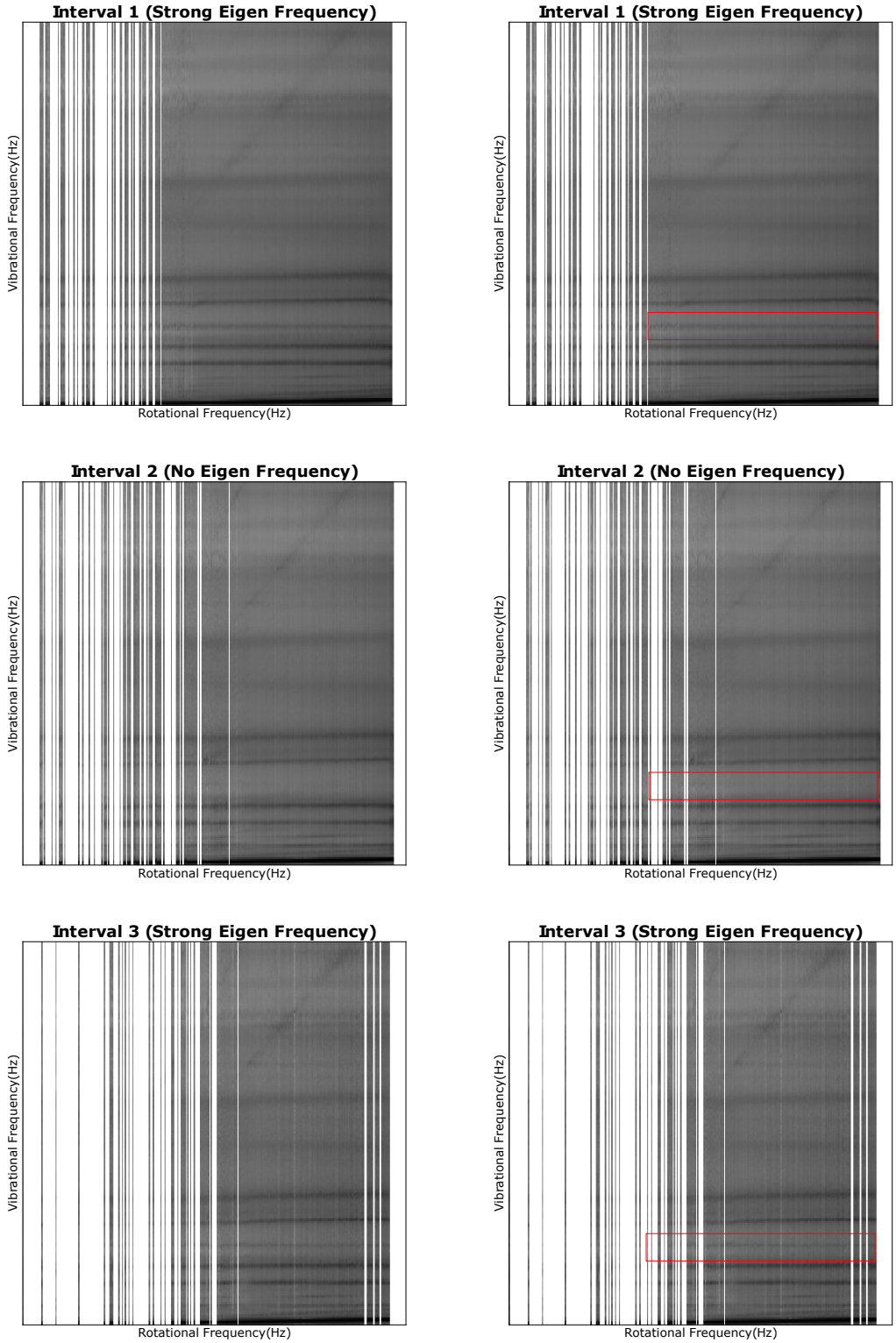

(a) Disappearance and reappearance of an eigen frequency across time.

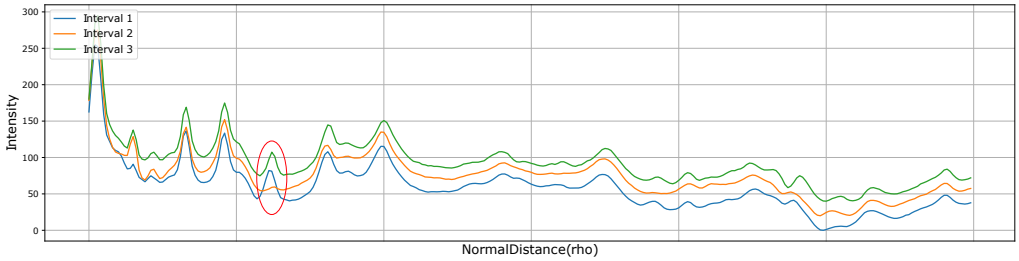

(b) Horizontal lined intensities for the three intervals.

Figure 4.4: Disappearance of a Natural Frequency

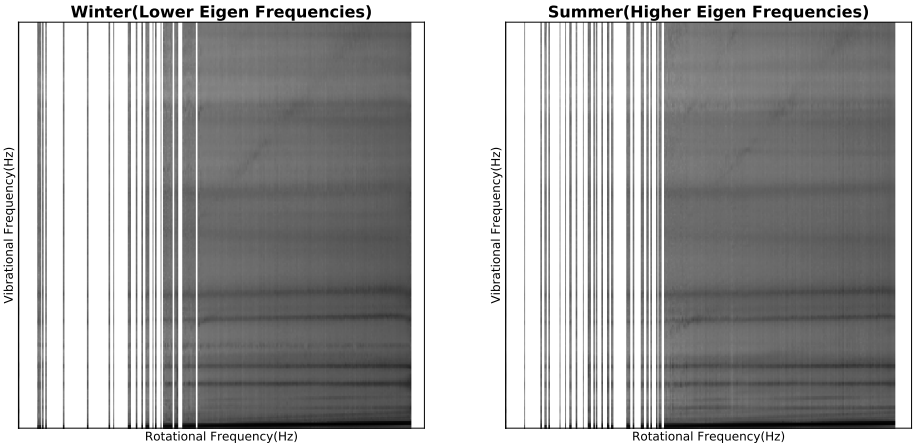

(a) Slight downward shift between Campbell diagrams of Winter and Summer.

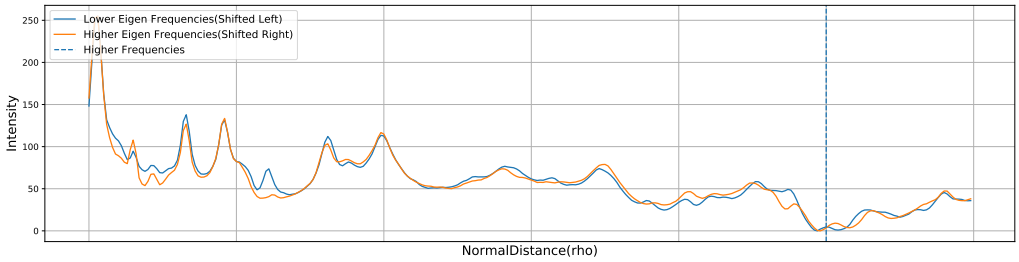

(b) Diagonal lines intensities for the two seasons.

Figure 4.5: Shifting Natural Frequencies

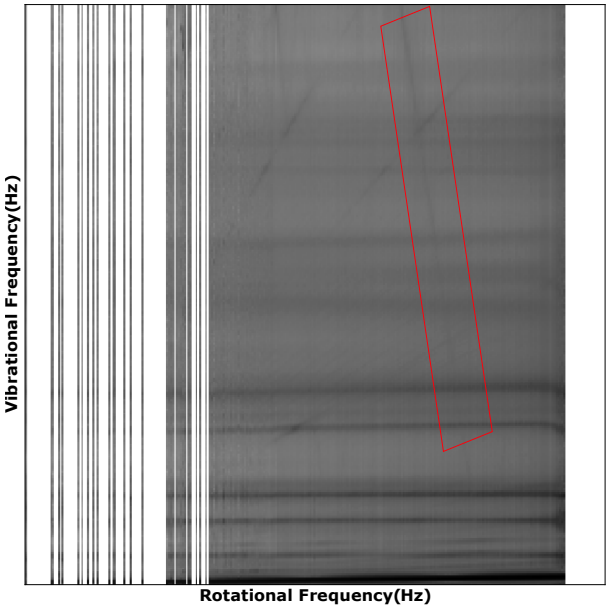

Figure 4.6: Campbell diagram with negative slope line.

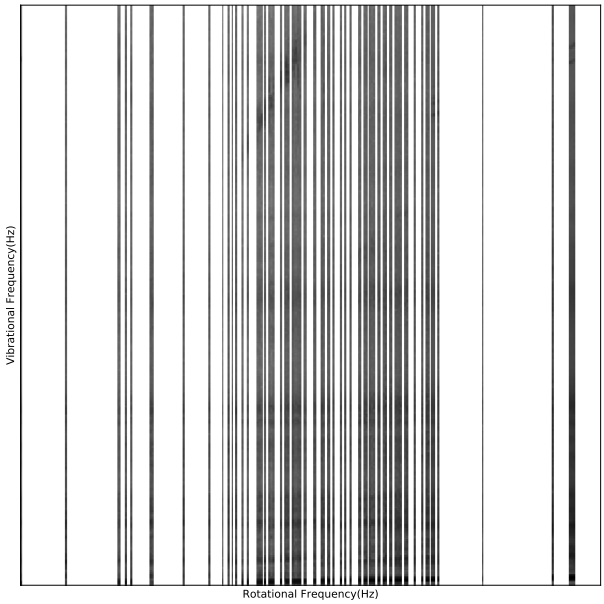

Figure 4.7: Sample Campbell diagram of one month for low vibrational frequencies.

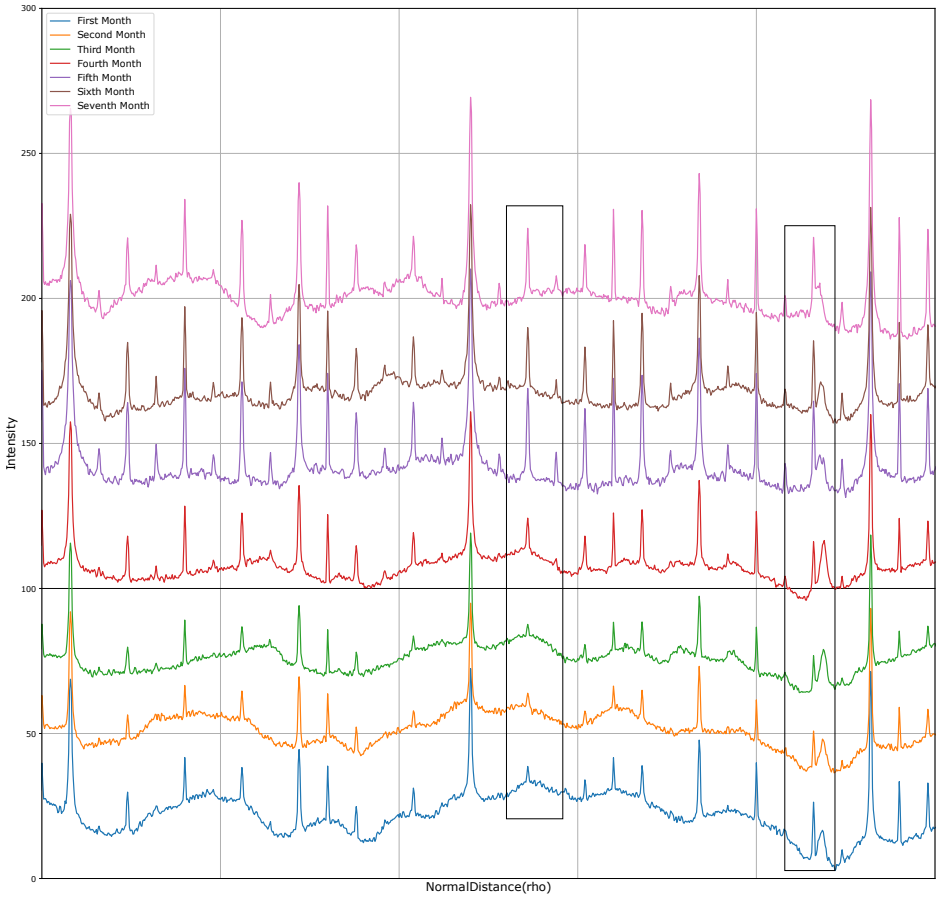

Figure 4.8: Horizontal lines intensities at high vibrational frequencies, using adjusted Radon transform, across months; intensities from each month is shifted upward from the previous month for better visualization. Some peaks appears starting in the second month and gets stronger across time, while other, already existing, peaks change shape

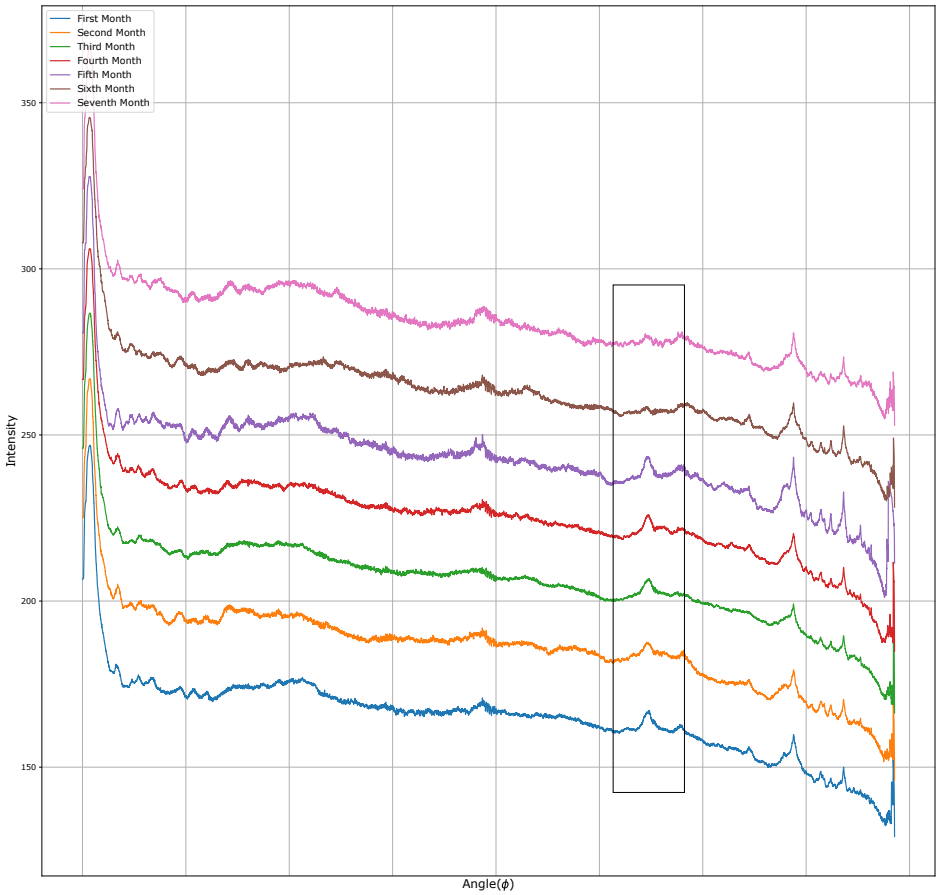

Figure 4.9: diagonal lines intensities, using adjusted Hough transform, across months; intensities from each month is shifted upward from the previous month for better visualization. A peak disappears when the damage is fixed.

Chapter 5

Conclusion

This thesis investigated two main research topics. The first one was line extraction in Campbell diagrams using Radon and Hough transforms. First, the effects of noise, which rendered the traditional edge detectors ineffective, were examined. Then, some adjustments were applied to the original Radon and Hough transforms to make them more suitable for the Campbell diagrams. It was concluded that these transforms can extract the lines in the Campbell diagrams with higher accuracy than the traditional gradient based edge detectors.

The second research topic was questioning the possibility of using Campbell diagrams as features for anomaly detection. Two data sets were examined for that purpose. The 25 WEP data set was analyzed visually to extract some of the interesting phenomena in the Campbell diagrams and to roughly determine the shortest time period to produce a useful Campbell diagram.
The anomaly data set was also analyzed visually to find the differences in the peaks in Radon and Hough transforms before the damage was reported and after it was fixed. Then wavelet transform was used to construct the Radon transform for the horizontal lines where the error between the constructed and the original signal was calculated and used as a criteria for determining the operation condition of the wind turbine. It can be concluded that Campbell diagrams can potentially be used as a feature for anomaly detection in the context of wind turbines.

The algorithmic analysis of Campbell diagrams are still in a premature phase, as all the previously presented results depend on the presence of a human observer in order to point the changes of the lines.
The suggested future step is to train a model in order to identify what changes in the Campbell diagrams correspond to serious events in the operation mode of the wind turbines, then build an algorithm that could capture the important changes as early as possible in order turn off the turbine before a serious damage occurs. Also the methods used, like wavelet transform, should be tested on other data sets in order to guarantee stability and accuracy.

Appendix A

Python Codes

A.1 Adjusted Radon Transform

```
import numpy as np
from skimage.transform._warps_cy import _warp_fast

def radon(image, theta=None, mode=1):
"""
This function implements an adjusted radon transform aiming to detect either
diagonal lines that pass through the origin or horizontal lines.
For detection of diagonal lines the image is rotated about the origin
(left lower corner not the center), and the pixels of column zero are added
and stored. For detection of horizontal lines the pixels of the image are
integrated along the horizontal axis.

:param image: 2-D array
      image in the form of array

:param theta: 1-D array
      the rotation angles in degrees.

:param mode: int
the type of detected lines either 1: detect diagonal lines
  2: detect horizontal lines

:return: 1d array of the intensities of the lines corresponding either
  to the rotation angles, or the distance from the origin.
"""

if theta is None:
theta = np.arange(0, np.pi/2, 0.0001)

if mode not in [1, 2]:
```

```
mode = 1

if mode == 1:
diagonal = np.ceil(np.sqrt((image.shape[0] ** 2) + (image.shape[1] ** 2)))
pad_width = [(0, int(diagonal - image.shape[0])), (image.shape[1], 0)]
padded_img = np.pad(image, pad_width, mode='constant', constant_values=0)

shift0 = np.array([[1, 0, -image.shape[1]],[0, 1, 0],[0, 0, 1]])
shift1 = np.array([[1, 0, image.shape[1]],[0, 1, 0],[0, 0, 1]])

def build_rotation(thetas):
r = np.array([[np.cos(thetas), np.sin(thetas), 0],
      [-np.sin(thetas), np.cos(thetas), 0],
      [0, 0, 1]])
return shift1.dot(r).dot(shift0)

lines = np.zeros(len(theta))

for i in range(len(theta)):
rotated = _warp_fast(padded_img, build_rotation(theta[i]))
lines[i] = rotated[:, image.shape[1]].sum(0)
lines[i] = lines[i]/(np.count_nonzero(rotated[:, image.shape[1]]))


else:
lines = image.sum(1)/np.count_nonzero(image, axis=1)


return lines
```

A.2 Adjusted Hough transform

```
import numpy as np

def hough(img, theta=None):
"""
This function implements an adjusted hough transform aiming to detect only
diagonal lines that pass through the origin.
For each non zero pixel in the image its intensity added to the accumulator
at the index corresponding to the angle the straight line, that passes with
this pixel, make with +ve x-axis

:param img:img: 2-D  image in the form of array

:param theta:1-D array of the rotation angles in degrees.

:return:1-D array of the normalized accumulator
"""

if theta is None:
theta = np.arange(np.pi/2, np.pi, 0.0001)

ctheta = np.cos(theta)
stheta = np.sin(theta)
accum = np.zeros((2, len(theta)))
x, y = np.where(img > 0)
for i in range(len(x)):
x_ = x[i]
y_ = y[i]
lin = np.round((ctheta * x_) + (stheta * y_))
accum[0, np.where(lin == 0)] += img[x_, y_]
accum[1, np.where(lin == 0)] += 1
norm = accum[0, :] / accum[1, :]

return norm
```

A.3 Shortest Time Period

```
import numpy as np
import pandas as pd
import matplotlib.pyplot as plt
from datetime import timedelta

def freq_inc(rotation_frequencies, start_freq=0.12, end_freq=0.23, bins=300, span=7):
"""
This method returns a data frame containing the percentage of frequencies,
in the input frequency range, included in intervals of length = span

Parameters
----------
rotation_frequencies: (,N) array-like
      the rotation frequencies

start_freq, end_freq : float, default: 0.12, 0.23
      the limits of the frequency range we are interested in.

bins  : int, default: 300
the number of bins to use for discretizing the rotor frequencies

span  : int, default: 7
the number of bins to use for discretizing the rotor frequencies
"""

clean_indices = ~np.isnan(rotation_frequencies)
rotation_frequencies = rotation_frequencies[clean_indices]

total_bins = np.linspace(0.00, max(rotation_frequencies.max(), 0.25), bins)
num_range_bins = int((end_freq - start_freq) * bins /
 (max(rotation_frequencies.max(),0.25)))
range_bins = np.digitize(np.linspace(start_freq, end_freq, num_range_bins),
total_bins)

start_date = np.arange(rotation_frequencies.index[0],
      rotation_frequencies.index[-1] - timedelta(days=span),
      timedelta(days=1), dtype=pd.Timestamp)
end_date = start_date + timedelta(days=span)
percentage = np.ndarray(shape=start_date.size)

for i in range(start_date.size):
rot_freq_span = rotation_frequencies[start_date[i]: end_date[i]]
non_empty_bins = np.digitize(rot_freq_span, total_bins)
```

```
intersection_set = np.intersect1d(non_empty_bins, range_bins)
percentage[i] = np.size(intersection_set) * 100 / num_range_bins

return pd.DataFrame({'Start Date': start_date, 'End Date': end_date,
'Intersection_Percentage': percentage})



import numpy as np
import pandas as pd

def shortest_interval(df_scada, least_percentage=80):
"""
This method calculate the shortest time period to produce a useful Campbell
diagram. A Campbell diagram is regarded useful if it contains a certain
percentage of frequencies.
:param df_scada:dataframe
  SCADA measurements fro 25 wind turbines
:param least_percentage:int
  Least percentace of operation frequencies in a useful campbell diagram
:return: 1D array of shortest time intervals for 25 wind turbines
"""

spans = np.zeros(25)
for wi in range(25):
span = 1
rotation_frequencies = df_scada[wi]['wep'+np.str(wi+1)+'/omega_mean']
flag = True
while flag:
df_perc = freq_inc(rotation_frequencies, span=span)
percentage = df_perc['Intersection_Percentage'].max()
if percentage >= least_percentage:
spans[wi] = span
flag = False
else:
span += 1

  return spans
```

A.4 Wavelet Transform

```
import numpy as np
import pywt

def wavelet_approx(Hl, wavelet, start=1000, end=5000,level=7):
```

```
"""
This method calculates the error between the Radon transform of the horizontal lines
in a campbell diagram and its approximation using wavelet transform.

:param Hl: Radon transform of the horizontal lines.
:param wavelet: Wavelet family.
:param start: starting index of the signal to be approximated.
:param end: ending index of the signal to be approximated.
:param level: Number of levels used in the approximation.
:return: Error
"""
if wavelet is None:
wavelet = pywt.Wavelet('sym5')
signal_len = end-start
max_level = pywt.dwt_max_level(signal_len, wavelet.dec_len)+1

coeffs = [0]*Hl.shape[0]
res = [0]*Hl.shape[0]
error = np.zeros(Hl.shape[0])

for i in range(Hl.shape[0]):
coeffs[i] = pywt.wavedec(Hl[i,start:end], wavelet,
 mode='symmetric', level=max_level)
res[i] = pywt.waverec(coeffs[i][:level+1] +
[None] * (max_level-level) , wavelet,
 mode='symmetric')
error[i] = (np.abs(Hl[0,start:end]-res[i][:signal_len])).sum()
return error
```

Bibliography

[BM94] P. M. Bentley and J. T. E. McDonnell. Wavelet transforms: an introduction. *Electronics Communication Engineering Journal*, 6(4):175–186, August 1994.

[Cha05] Venkata Ravikiran Chaganti. Edge detection of noisy images using 2-d discrete wavelet transform, 2005.

[Dea07] Stanley R. Deans. *The radon transform and some of its applications*. Dover Publications, Mineola, N.Y, 2007.

[Ehr08] Fredric F. Ehrich. Observations of Nonlinear Phenomena in Rotordynamics. *Journal of System Design and Dynamics*, 2(3):641–651, 2008.

[FP12] David Forsyth and Jean Ponce. *Computer vision: a modern approach*. Pearson, Boston, 2nd ed edition, 2012.

[Gen09] Giancarlo Genta, editor. *Vibration Dynamics and Control*. Mechanical Engineering Series. Springer US, Boston, MA, 2009.

[GHV04] M. van Ginkel, C. L. Luengo Hendriks, and L. J. van Vliet. *A short introduction to the Radon and Hough transforms and how they relate to each other*. 2004.

[Hau13] E. Hau. *Wind turbines: fundamentals, technologies, application, economics*. Springer, Heidelberg ; New York, third, translated edition edition, 2013.

[hou] Image Transforms - Hough Transform. `http://homepages.inf.ed.ac.uk/rbf/HIPR2/hough.htm`. Accessed: 2019-08-28.

[int] Integral transform. `https://en.wikipedia.org/w/index.php?title=Integral_transform&oldid=912613582`. Accessed: 2019-08-28.

[Mal09] S. G. Mallat. *A wavelet tour of signal processing: the sparse way*. Elsevier/Academic Press, Amsterdam ; Boston, 3rd ed edition, 2009.

[MMH17] Kishan G. Mehrotra, Chilukuri K. Mohan, and HuaMing Huang. *Anomaly Detection Principles and Algorithms*. Terrorism, Security, and Computation. Springer International Publishing, Cham, 2017.

[Rad86] J. Radon. On the determination of functions from their integral values along certain manifolds. *IEEE Transactions on Medical Imaging*, 5(4):170–176, December 1986.

[RHB06] K. F. Riley, M. P. Hobson, and S. J. Bence. *Mathematical methods for physics and engineering*. Cambridge University Press, Cambridge ; New York, 3rd ed edition, 2006. OCLC: ocm62532900.

[SKN16] M. Sornam, M. S. Kavitha, and M. Nivetha. Hysteresis thresholding based edge detectors for inscriptional image enhancement. In *2016 IEEE International Conference on Computational Intelligence and Computing Research (ICCIC)*, pages 1–4, December 2016.

[Smi15] Julius O. Smith. *Mathematics of the Discrete Fourier Transform (DFT)*. `http://ccrma.stanford.edu/~jos/mdft/`, accessed (2019-08-15). online book, 2007 edition.

[ZS17] Arthur Zimek and Erich Schubert. Outlier Detection. In Ling Liu and M. Tamer Özsu, editors, *Encyclopedia of Database Systems*, pages 1–5. Springer, New York, NY, 2017.